Fluorescence in Quantum Dynamics: Accurate Spectra Require Post-Mean-Field Approaches

Carlos M. Bustamante,[1] Esteban D. Gadea,[1] Tchavdar N. Todorov,[2] Andrew Horsfield,[3] Lorenzo Stella,[4,5] and Damian A. Scherlis[1]

[1)] *Departamento de Química Inorgánica, Analítica y Química Física/INQUIMAE, Facultad de Ciencias Exactas y Naturales, Universidad de Buenos Aires, Buenos Aires (C1428EHA) Argentina*

[2)] *Centre for Quantum Materials and Technologies, School of Mathematics and Physics, Queen's University Belfast, Belfast BT7 1NN, United Kingdom*

[3)] *Department of Materials, Thomas Young Centre, Imperial College London, South Kensington Campus, London, SW7 2AZ, United Kingdom*

[4)] *Centre for Light-Matter Interactions, School of Mathematics and Physics, Queen's University Belfast, Belfast BT7 1NN, United Kingdom*

[5)] *School of Chemistry and Chemical Engineering, Queen's University Belfast, Belfast BT9 5AG, United Kingdom*

(*Electronic mail: t.todorov@qub.ac.uk)

(*Electronic mail: cbustamante@qi.fcen.uba.ar)

(Dated: 9 March 2023)

Real time modelling of fluorescence with vibronic resolution entails the representation of the light-matter interaction coupled to a quantum-mechanical description of the phonons, and is therefore a challenging problem. In this work, taking advantage of the difference in time-scales characterizing internal conversion and radiative relaxation—which allows us to decouple these two phenomena by sequentially modelling one after the other—we simulate the electron dynamics of fluorescence through a master equation derived from the Redfield formalism. Moreover, we explore the use of a recent semiclassical dissipative equation of motion [*Phys. Rev. Lett.* **126**, 087401 (2021)], termed CEED, to describe the radiative stage. By comparing the results with those from the full quantum-electrodynamics treatment, we find that the semiclassical model does not reproduce the right amplitudes in the emission spectra when the radiative process involves the deexcitation to a manifold of closely lying states. We argue that this flaw is inherent to any mean-field approach, and is the case with CEED. This effect is critical for the study of light-matter interaction and this work is, to our knowledge, the first one to report this problem. We note that CEED reproduces the correct frequencies in agreement with quantum electrodynamics. This is a major asset of the semiclassical model, since the emission peak positions will be predicted correctly without any prior assumption about the nature of the molecular Hamiltonian. This is not so for the quantum electrodynamics approach, where access to the spectral information relies on knowledge of the Hamiltonian eigenvalues.

I. INTRODUCTION

The phenomenon of fluorescence is usually understood in terms of the picture illustrated in Figure 1. In this picture we differentiate three stages: i) excitation, ii) thermal relaxation and iii) radiative decay. We note that the emission frequency is lower than the absorption frequency, an effect known as the Stokes shift[1]. Despite the simplicity of this picture, the last two stages of this process are not trivial to describe theoretically since they require a description of the molecular environment, including all vibrational degrees of freedom and the solvent, if present.

Thermal relaxation involves the interaction between the system and a vibrational bath. A common strategy for simulating this process is to use non-adiabatic excited-state dynamics. In the literature there are many different approaches to this problem within an *ab initio* framework[2,3]. The most popular methods include semi-classical approaches such as Ehrenfest Dynamics and Surface Hopping, usually in a multiscale QM/MM (Quantum Mechanics / Molecular Mechanics) framework to describe the environment in a classical and computationally less expensive way[4,5]. Despite advances in these methodologies, it is difficult to avoid their inherently high computational cost. A full quantum dynamics representation (QD) is a more accurate and natural framework to describe the evolution of the vibrational bath[6,7]. Even though the computational cost of this methodology increases exponentially with the number of degrees of freedom, it is possible to reduce the complexity by working with simple and parameterized models. These kinds of models are frequently cheaper and sufficiently accurate for conceptual studies. They also offer a more intuitive and understandable way to study phenomena such as energy transfer[8], photoisomerization[9,10], and fluorescence[11]. Moreover, these models allow conceptual studies in the framework of time-resolved spectroscopy[12].

The following stage in the relaxation process is the radiative decay, and its description is also challenging. The most accurate, but expensive, way to do this is by the use of quantum electrodynamics (QED). Efforts to include this methodology in *ab initio* calculations led to the development of quantum electrodynamics density functional theory (QEDFT)[13,14], and coupled-cluster electrodynamics[15], however the computational cost is high. Semi-classical methods are a numerically cheaper alternative; these include Ehrenfest dynamics, Maxwell-Bloch equations, and optical Bloch equations, to mention just a few[16]. One limitation of these method-

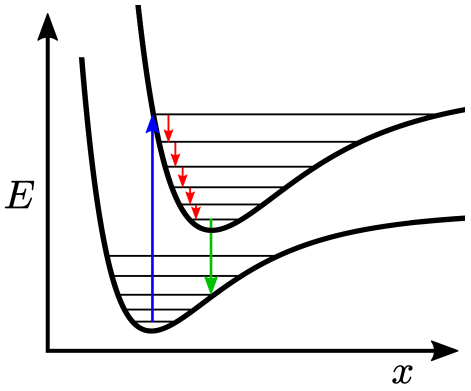

FIG. 1. Fluorescence description using two one-dimensional potential energy surfaces. The process starts with the excitation of the system (blue arrow), continues with thermal relaxation (red arrows) and finishes with radiative decay (green arrow).

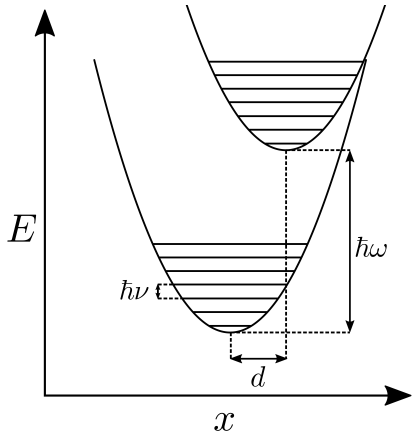

FIG. 2. Two-level system represented as two harmonic surfaces. Both oscillators have the same angular frequency ($\hbar\nu$) but different minima shifted by an amount d.

ologies is that they cannot model spontaneous emission of phonons, though this was overcome by the development of Ehrenfest+R[17]. A second limitation is that the transferability of these methodologies is not always a simple task. As a midpoint solution to this problem, we recently introduced a semi-classical approach called CEED (Coherent Electron Electric-field Dynamics), which, while it does not include spontaneous emission, has proven versatile, low-cost and able to offer a good description of radiative dissipation in *ab initio* electron dynamics. We note it has no adjustable parameters and is adaptable to any level of theory[18,19]. Despite their differences, all these semi-classical methodologies share the same mean-field spirit, including some *ab initio* approaches such as the Maxwell–Pauli–Kohn–Sham equations (MPKS) obtained from QEDFT in the mean-field limit[20].

In this work we present a general scheme based on CEED to describe light emission in simple fluorescent models, evaluating the performance and limitations of our semi-classical methodology. These fluorescent systems are described by vibronic states which are propagated using QD. In order to simulate the thermal relaxation we make use of the Redfield formalism[21] to describe a quantum bath of harmonic oscillators. In section II we show results obtained in two simple models using harmonic and anharmonic vibrational modes. In section III we discuss the origin of key discrepancies with the full QED description. We finish with section IV where we present conclusions and perspectives for our approach that also apply to other mean-field methodologies.

II. SIMULATING FLUORESCENCE

A. The harmonic case

The molecular model that we use for our first test is depicted in Figure 2. It is a two-level system (TLS), with a ground state $|g\rangle$ and an excited state $|e\rangle$. The excited level is coupled to a harmonic oscillator of angular frequency ν, producing two shifted parabolic surfaces of equal stiffness, with a spatial shift d. The corresponding Hamiltonian is

$$\hat{H}_{\text{mol}} = \left(\hbar\omega + \hbar\nu Q - \hbar\nu\sqrt{Q}\left(\hat{a}^\dagger + \hat{a}\right)\right)|e\rangle\langle e| + \hbar\nu\left(\hat{a}^\dagger\hat{a} + \frac{1}{2}\right) \tag{1}$$

where $\hbar\omega$ is the energy gap between the minima of the electronic energy surfaces, M is the mass of the oscillator, $Q = \frac{M\nu}{2\hbar}d^2$, and $\hat{a}^\dagger$ and $\hat{a}$ are the creation and annihilation operators of the harmonic oscillator. To include vibrational relaxation we couple the vibrational modes of our molecular system to a phonon bath, represented by the Hamiltonian

$$\hat{H} = \hat{H}_{\text{mol}} + \sum_j \hbar\nu_j\left(\hat{b}_j^\dagger\hat{b}_j + \frac{1}{2}\right) - K_0\hat{X}\sum_j \hat{X}_j \tag{2}$$

where $\hat{X} = \sqrt{\frac{\hbar}{2M\nu}}\left(\hat{a}^\dagger + \hat{a}\right)$, and the index j labels the degrees of freedom of the bath. The bath vibrational mode j has angular frequency ν_j, and raising and lowering operators $\hat{b}_j^\dagger$ and $\hat{b}_j$. For the sake of simplicity, we have used the same mass M for the molecular vibration and for the phonon bath. Following the Redfield formalism, it is possible to derive the following master equation for the evolution of the reduced molecular density operator

$$\mathrm{i}\hbar\frac{d\hat{\rho}(t)}{dt} = \left[\hat{H}_{\text{mol}}, \hat{\rho}(t)\right] - \left[\hat{X}, \left(\left[\hat{\chi}^{(1)}, \hat{\rho}(t)\right] + \left\{\hat{\chi}^{(2)}, \hat{\rho}(t)\right\}\right)\right], \tag{3}$$

The matrix elements of $\hat{\chi}^{(1)}$ and $\hat{\chi}^{(2)}$ are defined in terms of the eigenstates $|i\rangle$ of the system,

$$\begin{aligned}\chi_{ij}^{(1)} &= \frac{\mathrm{i}\pi X_{ij}K_0^2(2N(|\omega_{ij}|)+1)}{4M|\omega_{ij}|\Delta\omega},\\ \chi_{ij}^{(2)} &= -\frac{\mathrm{i}\pi X_{ij}K_0^2}{4M\omega_{ij}\Delta\omega},\end{aligned} \tag{4}$$

where $X_{ij} = \langle i|\hat{X}|j\rangle$, $\hbar\omega_{ij} = E_i - E_j$ and $\Delta\omega = \omega_{\max} - \omega_{\min}$, being E_i the energy of the eigenstate i, and $\omega_{\max}$ and $\omega_{\min}$

TABLE I. Molecular and bath parameters.

Parameter	Value
$\hbar\omega$	1.63 eV
$\hbar\nu$	0.11 eV
K_0	3.37 eV/Å^2
M	10.0 AMU
ω_{min}	0.054 eV
ω_{max}	0.163 eV
T	0.0 K
d	0.13 Å

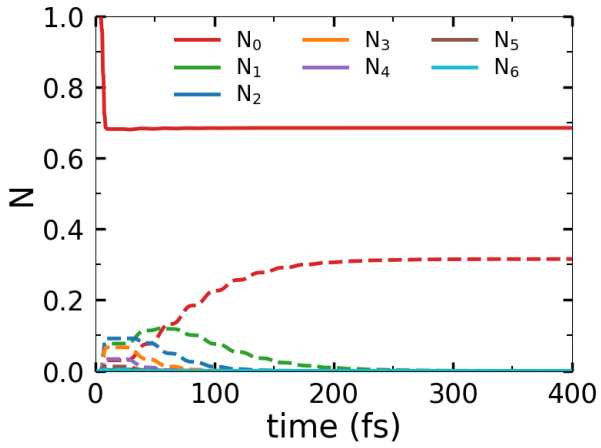

FIG. 3. Evolution of the vibrational occupations of the ground (full line), and excited (dashed lines) states, after the application of the laser pulse.

the maximum and minimum frequencies of the bath respectively. The derivation of these terms, the master equation and its relation with the standard Redfield equation can be found in Appendix A. The parameters used for our first test calculations are given in Table I. Initially the system occupies the state $|g,0\rangle$ (where the first index indicates the electronic state and the second one the vibrational quantum number) and is then perturbed by a laser pulse. This stage is modelled by the following Hamiltonian

$$\begin{aligned}\hat{H} &= \hat{H}_{\text{mol}} - E_x(t)\hat{\mu}_x \\ &= \hat{H}_{\text{mol}} - eE_x(t)\left(\hat{X}-\hat{x}\right).\end{aligned} \tag{5}$$

This new term corresponds to the laser, where $\hat{x} = x_{eg}\hat{\sigma}_x$, $\hat{\sigma}_x = |e\rangle\langle g| + |g\rangle\langle e|$, and the electric field $E_x(t) = E_0\cos(\omega_0(t-t_0))e^{-\left(\frac{t-t_0}{\sigma}\right)^2}$, with $\hbar\omega_0 = 1.85$ eV, $\sigma = 1.21$ fs, $t_0 = 6.05$ fs, and $E_0 = 0.514\ V\text{Å}^{-1}$. After the initial perturbation ($t = 24.2$ fs), the system evolves according to Equation 3, which describes the vibrational relaxation. In Figure 3 we see how the occupation of state $|g,0\rangle$ decreases during the duration of the pulse, and how this density transitions to the states $|e,j\rangle$ corresponding to a coherent state on the upper energy surface. Thereafter, equation 3 induces the thermalization of the excited density down to the state $|e,0\rangle$, in approximately 250 fs. The bath does not include high frequency modes so it is

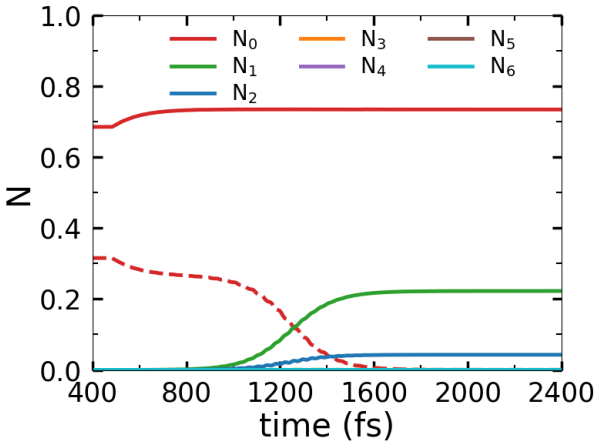

FIG. 4. Evolution of the vibrational occupations of the ground state (full lines), and excited state (dashed line), after the thermalization and during the radiative decay driven by the CEED Hamiltonian, with $K_a = 5.0\times10^7$.

decoupled from electronic transitions. Because of this, the vibrational degrees of freedom thermalize to $T = 0$ K, with no further relaxation.

At $t = 480$ fs, when we consider the stationary state converged enough, the phonon bath is turned off. From then on, we evolve the density under the CEED Hamiltonian[18,19] to include the radiative emission

$$i\hbar\frac{d\hat{\rho}}{dt} = [\hat{H}_{\text{mol}},\hat{\rho}] + K_a\frac{e\mu_0}{i6\pi c\hbar}\langle\ddot{\mu}\rangle\left[\left[\hat{x},\hat{H}_{\text{mol}}\right],\hat{\rho}\right], \tag{6}$$

where the numerical factor K_a is included to accelerate the dissipation and let the system reach the ground state within an accessible simulation time[18]. The decay time of this process is usually in the order of nanoseconds. With the help of K_a this time is artificially reduced to hundreds of femtoseconds. We assume here that the difference in time-scales between thermal relaxation and radiative emission is large enough to treat them as separate, uncoupled processes. Figure 4 shows how the vibrational occupations change during the radiative decay driven by Equation 6. We can see how the excited state empties completely as the ground state occupations grow. The final occupations after the emission can be compared with the expected values predicted by the Franck-Condon principle (FCP) and the Fermi Golden Rule (FGR). In Figure 5 we can see the differences between the expected and final occupations obtained from the CEED Hamiltonian. The differences converge as K_a decreases: in particular, the final populations are insensitive to the acceleration factor when this is smaller than 3×10^7. As it was already shown in previous works[18,19], CEED depends on the coherences among the electronic states. At the same time, these coherences are affected by the dynamics of the wave packet which oscillates in the ground state as the system decays radiatively. When the decay rate is in the order of the oscillation frequency of the lower state (which may occur for large values of K_a), the oscillation affects the relative decay rates among the states and the final occupations. This effect is no longer relevant as K_a decreases since in that

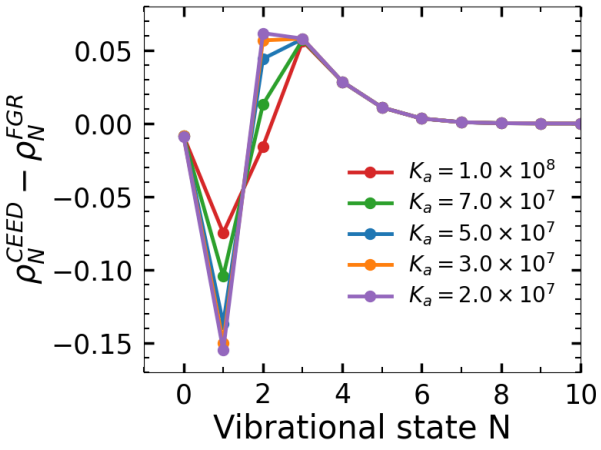

FIG. 5. Difference between the expected and the obtained final occupations by CEED with different values of K_a.

situation the dynamics depends on the evolution of the occupations and not on the coherences.[19] This is the case for the value of K_a that we used in all our simulations. Nevertheless, we see that the first two occupations are overestimated and the higher occupations are underestimated despite the convergence of K_a (Figure 5). The differences are small, of 15% or less. However, Figure 5 indicates that even though CEED describes fluorescence qualitatively, part of the physics is not well represented. The next section sheds light on this.

Our approach allows us to obtain the spectral density $S(t,\omega)$ of the time-dependent dipole moment for a specific stretch of the dynamics centered on time t and extending from $t - T/2$ to $t + T/2$:[22]

$$S(t,\omega) = \int_{t-T/2}^{t+T/2} C(t,\tau) e^{-i\omega\tau} d\tau, \tag{7}$$

with $C(t,\tau)$ being, in our case, the classical time-correlation function associated with time t, calculated here as

$$C(t,\tau) = [\mu(t) - \langle\mu\rangle(t)] \times [\mu(t+\tau) - \langle\mu\rangle(t)], \tag{8}$$

where the dynamical dipole is measured relative to its average value on the same interval, $\langle\mu\rangle$. Thus $S(t,\omega)$ reflects the spectra for different stages around time t. Depending on the stage, the result corresponds to the absorption or emission spectrum. Figure 6 shows $S(t,\omega)$ at different times during the simulations depicted in Figure 3 and 4. For $t < 480$ fs we get the absorption spectrum of the system. The band amplitudes decrease as the system thermally relaxes. At $t = 300$ fs only the absorption peak of lowest frequency survives, corresponding to the transition $|g,0\rangle \rightarrow |e,0\rangle$. For $t > 480$ fs, new peaks appear corresponding to the emission process. Their amplitudes also decrease as the electronic relaxation continues, but the spectrum shape is constant as it is expected. Since we do not include the thermal relaxation after the radiative emission the vibrational frequency keeps appearing in the spectrum at low frequencies, but this has no effect on the fluorescence spectrum. About the position of the peaks (frames with $t = 1300$ fs or $t = 1600$ fs of Figure 6), they agree with some of the expected emission frequencies for this system. However, as we have already seen for the case of the final occupations, the relative amplitudes of the emission frequencies do not follow the expected distribution according to the FCP. Figure 7 shows these drastic differences among the relative intensities.

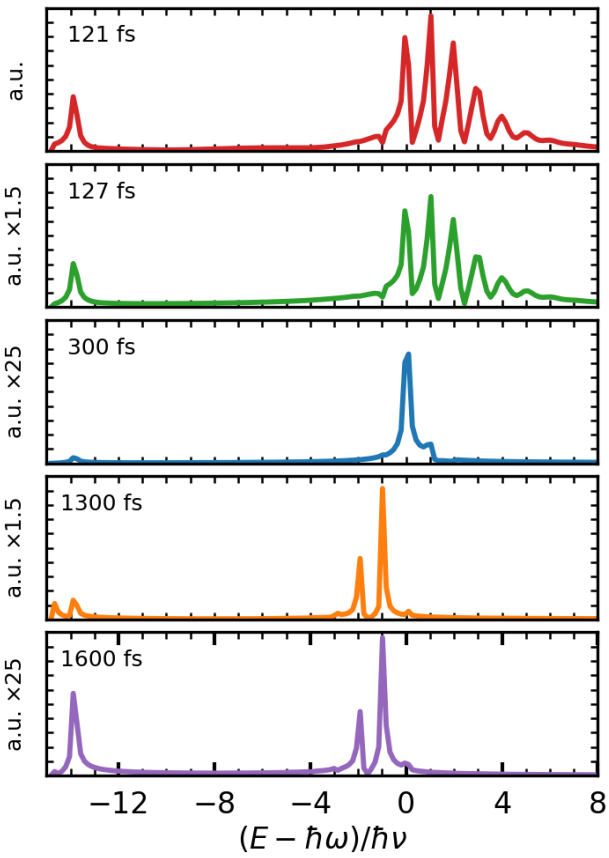

FIG. 6. Spectral density for different times along the dynamics ($K_a = 5.0 \times 10^7$ in Eq. 6). The horizontal axis represents the transition energy relative to $\hbar\omega$ and scaled by $\hbar\nu$

B. The anharmonic case

For our second test, we considered a more realistic case. We use the same molecular Hamiltonian, but now we include the interaction between the two energy surfaces, giving place to anharmonicity:

$$\begin{aligned}\hat{H}_{mol} = &\left(\hbar\omega + \hbar\nu Q - \hbar\nu\sqrt{Q}\left(\hat{a}^\dagger + \hat{a}\right)\right)|e\rangle\langle e| - \tau\hat{\sigma}_x \\ &+ \hbar\nu\left(\hat{a}^\dagger\hat{a} + \frac{1}{2}\right).\end{aligned} \tag{9}$$

Table II shows the parameters used for this case. These are similar to those used by Giavazzi *et al*[11]. The system was excited with a similar electric pulse as adopted in the first test, but now $\omega_0 = 2.73$ eV and $E_0 = 0.771$ eV/Å^{-1}. We used the same protocol and activation times for the bath and CEED.

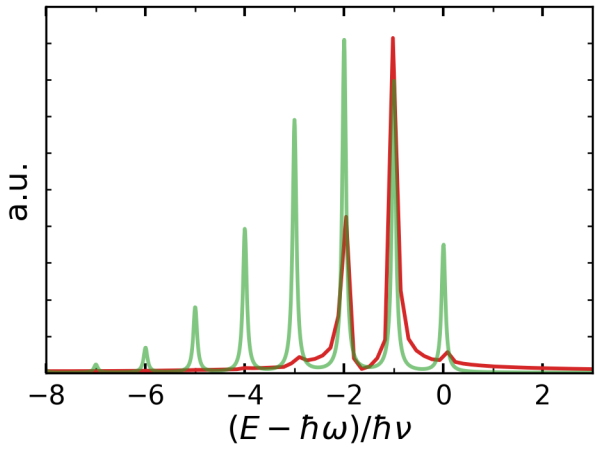

FIG. 7. Spectral density at $t = 1300$ fs from Figure 6 (red), compared with the expected intensities (green), according to FCP.

TABLE II. Molecular and bath parameters for the anharmonic system.

Parameter	Value
$\hbar\omega$	1.824 eV
$\hbar\nu$	0.172 eV
K_0	6.74 eV/Å^2
M	10.0 UMA
ω_{min}	0.086 eV
ω_{max}	0.258 eV
T	0.0 K
d	0.11 Å
τ	0.88 eV

Again we use the Fourier transform of the correlation function to get the spectrum resolved in time (Figure 8). Now we keep observing an intense peak after the thermal dissipation. It corresponds to the minimum absorption frequency and continues after the relaxation due the coherence between the ground and the excited states. For $t > 480$ fs, after the activation of CEED, this peak loses intensity, and new peaks appear because of the emission process. In Figure 8 we see the fluorescence spectrum at 739 fs. The main peak is located at 2.39 eV and other two less intense ones appear at 2.55 eV and 2.22 eV. Again, the amplitudes do not correspond to the expected distribution according to FCP (Figure 9). And once more, we observe an intense attenuation of peaks far from the main transitions.
In previous works[18,19], we showed that CEED respects the selection rules during the relaxation. In fact, the missing peaks in the emission spectrum are not absent but attenuated, a consequence of big differences on the decay rates for each transition.

III. COMPARING QED AND CEED

In order to understand the reason for the observed discrepancies in this section we will work in the length gauge with

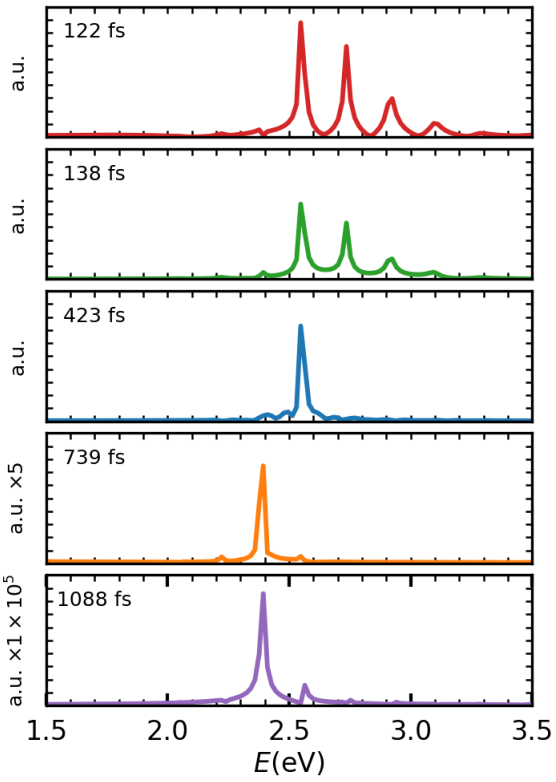

FIG. 8. Spectral density at different times, for the anharmonic system ($K_a = 5.0 \times 10^7$ in Eq. 6).

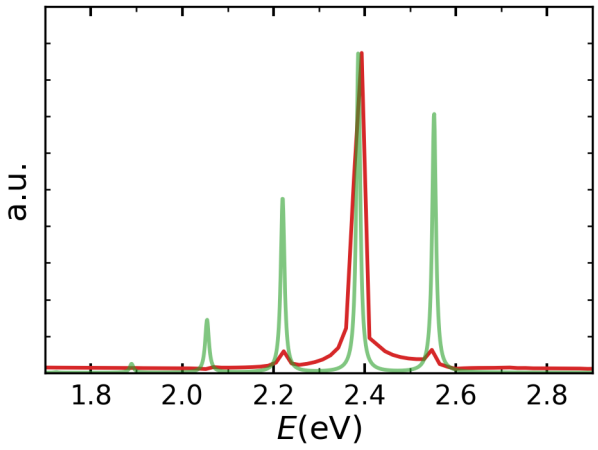

FIG. 9. Spectral density at $t = 739$ fs from Figure 8 (red), compared with the expected intensities (green) according to FCP.

the non-relativistic QED Hamiltonian

$$\hat{H} = \hat{H}_{\text{mol}} + \sum_{\mathbf{k}} \hbar\omega_{\mathbf{k}} \left(\hat{N}_{\mathbf{k}} + \frac{1}{2} \right) - \sum_{\mathbf{k}} \hat{\mathbf{E}}_{\mathbf{k}} \cdot \hat{\boldsymbol{\mu}}, \qquad (10)$$

where $\hat{N}_{\mathbf{k}}$ is the occupation operator of the photon with wave vector $\mathbf{k} = (k_x, k_y, k_z)$ and with its corresponding frequency $\omega_{\mathbf{k}} = ck$. $\hat{\boldsymbol{\mu}}$ is the electronic dipole moment operator and $\hat{\mathbf{E}}_{\mathbf{k}}$ is the photon electric field operator, which can be expanded as

a function of the photon creator and annihilator operators ($\hat{a}^\dagger$, $\hat{a}$)

$$\hat{\mathbf{E}}_{\mathbf{k}} = -\mathrm{i}\sum_{\lambda=1}^{2} \epsilon_{\mathbf{k},\lambda}\left(\frac{\hbar\omega_{\mathbf{k}}}{2\varepsilon_0 V}\right)^{1/2}(\hat{a}^\dagger_{\mathbf{k},\lambda} - \hat{a}_{\mathbf{k},\lambda}), \tag{11}$$

where V is the normalisation volume and we have considered the dipole approximation, $e^{\mathbf{ik}\cdot\mathbf{r}} \approx 1$.
Again, we can use the Redfield formalism to obtain the master equation for the evolution of the reduced molecular density operator using the Hamiltonian of Equation 10

$$\mathrm{i}\hbar\frac{d\hat{\rho}}{dt} = [\hat{H}_{\mathrm{mol}}, \hat{\rho}] + e[\hat{x}, ([\hat{\chi}^{(1)}, \hat{\rho}] + \{\hat{\chi}^{(2)}, \hat{\rho}\})], \tag{12}$$

where $\hat{x}$ is the position operator, and now the matrix elements of the operators $\hat{\chi}^{(1)}$ and $\hat{\chi}^{(2)}$ are

$$\begin{aligned}\chi^{(1)}_{ij} &= -\frac{\mathrm{i}ex_{ij}|\omega_{ij}|^3}{12\pi\varepsilon_0 c^3}(2N(|\omega_{ij}|)+1)\\ \chi^{(2)}_{ij} &= \frac{\mathrm{i}ex_{ij}\omega^3_{ij}}{12\pi\varepsilon_0 c^3}.\end{aligned} \tag{13}$$

where now $N(|\omega_{ij}|)$ is the occupation of the photon mode with frequency $|\omega_{ij}|$ at temperature T. The derivation of these terms and the master equation can be found in Appendix B
On the other hand we have the Liouville equation combined with the CEED Hamiltonian, now without the factor of K_a:

$$\mathrm{i}\hbar\frac{d\hat{\rho}}{dt} = [\hat{H}_{\mathrm{mol}}, \hat{\rho}] + \frac{e\mu_0}{\mathrm{i}6\pi c\hbar}\langle\ddot{\mu}\rangle\left[\left[\hat{x}, \hat{H}_{\mathrm{mol}}\right], \hat{\rho}\right]. \tag{14}$$

A straightforward comparison between Equations 12 and 14 can be done by studying the evolution of the occupations, i.e., the diagonal elements of the density matrix, ρ_{jj}. This analysis is greatly simplified by noting that the characteristic frequencies of the diagonal elements are much lower than those of the off-diagonal elements, which allows for averaging out over fast modes to obtain rate equations. In ref.[19] (see Equation 10 and the Appendix in that paper) the following relation is derived from Eq. 14:

$$\frac{d\rho_{jj}}{dt} = \frac{e^2}{3\pi\varepsilon_0 c^3\hbar}\rho_{jj}\sum_k \rho_{kk}\omega^3_{kj}|x_{kj}|^2. \tag{15}$$

Using the same approach, it is possible to start from Equation 12 to get:

$$\frac{d\rho_{jj}}{dt} = \frac{e^2}{3\pi\varepsilon_0 c^3\hbar}\left(\sum_{k<j}\rho_{jj}\omega^3_{kj}|x_{kj}|^2 + \sum_{k>j}\rho_{kk}\omega^3_{kj}|x_{kj}|^2\right), \tag{16}$$

If we consider the simplest case where the transition involves one initial excited state i and one final ground state f, we get from equation 16 the FGR behavior:

$$\frac{d\rho_{ii}}{dt} = -\frac{e^2}{3\pi\varepsilon_0 c^3\hbar}\omega^3_{if}|x_{if}|^2\rho_{ii}, \tag{17}$$

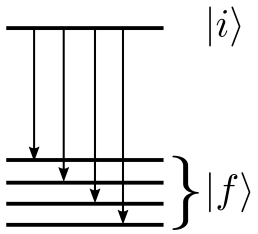

FIG. 10. Transition from one initial $|i\rangle$ state to many final states $|f\rangle$

while from Equation 15 the result is

$$\begin{aligned}\frac{d\rho_{ii}}{dt} &= -\frac{e^2}{3\pi\varepsilon_0 c^3\hbar}\omega^3_{if}|x_{if}|^2\rho_{ii}\rho_{ff}\\ &= -\frac{e^2}{3\pi\varepsilon_0 c^3\hbar}\omega^3_{if}|x_{if}|^2\rho_{ii}(1-\rho_{ii}).\end{aligned} \tag{18}$$

As shown in[18,19], when the initial state is almost empty the rate equation obtained from CEED closely reproduces the FGR result. This agreement is also achieved if the transition goes sequentially from one state to another. Once the upper state is almost empty, the decay follows an exponential rate which agrees with FGR.[18]
We now consider a different scenario relevant to fluorescence. Fluorescent processes usually imply the transition from a given initial state i to a multiplet of final states f, where the energy difference between the initial and final states is much larger than the energy differences between the possible final states (Figure 10). With this in mind, and assuming for argument's sake that the transition matrix elements x_{if} are comparable for different final states, we can write Equation 16 as

$$\begin{aligned}\frac{d\rho_{ii}}{dt} &\approx -\frac{e^2}{3\pi\varepsilon_0 c^3\hbar}\rho_{ii}\sum_f \omega^3_{if}|x_{if}|^2\\ &= -\frac{N_f e^2}{3\pi\varepsilon_0 c^3\hbar}\omega^3_{if}|x_{if}|^2\rho_{ii},\end{aligned} \tag{19}$$

where N_f is the number of final states. Equation 15 by contrast becomes

$$\begin{aligned}\frac{d\rho_{ii}}{dt} &\approx -\frac{e^2}{3\pi\varepsilon_0 c^3\hbar}\omega^3_{if}|x_{if}|^2\rho_{ii}\sum_f \rho_{ff}\\ &= -\frac{e^2}{3\pi\varepsilon_0 c^3\hbar}\omega^3_{if}|x_{if}|^2\rho_{ii}(1-\rho_{ii}).\end{aligned} \tag{20}$$

Even though this last expression predicts the exponential decay when the initial state is almost unoccupied, the decay constant is suppressed by a factor of N compared with the QED prediction. The differences turn out to be larger if the simplifying assumptions are removed. Equation 16 still describes an exponential decay,

$$\frac{d\rho_{ii}}{dt} = -\frac{e^2}{3\pi\varepsilon_0 c^3\hbar}\rho_{ii}\sum_f \omega^3_{if}|x_{if}|^2, \tag{21}$$

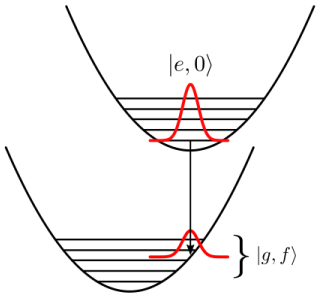

FIG. 11. Transition process from one energy surface to a lower one, involving two coherent states represented with red curves.

but Equation 15 describes a more complex dynamics,

$$\frac{d\rho_{ii}}{dt} = -\frac{e^2}{3\pi\varepsilon_0 c^3\hbar}\rho_{ii}\sum_f \rho_{ff}\omega_{if}^3|x_{if}|^2, \tag{22}$$

where $\rho_{ff} < 1$, which implies that the decay rate predicted by CEED is again lower than the one predicted by QED.
Particularly, we are interested in the case depicted in Figure 11. Here the deexcitation involves two coherent states, as expected during a vertical transition. In this case, we have that $\rho_{ff} \propto |x_{if}|^2$. According to Equation 16, the evolution of the occupations of the final states depend only on the occupation of the initial state:

$$\frac{d\rho_{ff}}{dt} = \frac{e^2}{3\pi\varepsilon_0 c^3\hbar}\omega_{if}^3|x_{if}|^2\rho_{ii}. \tag{23}$$

By contrast, Equation 15 gives the following expression for the evolution of the final states:

$$\frac{d\rho_{ff}}{dt} \propto \frac{e^2}{3\pi\varepsilon_0 c^3\hbar}\omega_{if}^3|x_{if}|^4\rho_{ii}, \tag{24}$$

where now the population rate of each final state depends on $|x_{if}|^4$.
These differences in the decay rates can explain the drastic differences observed in the emission spectrum. Comparing Equation 21 with Equation 22, it is possible to say that CEED decay rates are weighted by the occupations of the final states. Apparently, these weights affect in the same way the transition terms $|x_{ij}|^2$ involved in the amplitude of the spectral lines. In this way, the faster the states are occupied the higher the spectral signal.

IV. COMMENTS AND CONCLUSION

In this work we explored the use of CEED, a semiclassical equation of motion to model energy dissipation associated with radiative decay, to describe fluorescence in two simple molecular models. The comparison with full QED simulations exposed incorrect modelling of fluorescence when mean-field light-matter interaction is used. The Appendix C demonstrates that CEED is a mean-field light-matter theory akin to Ehrenfest dynamics: our model underestimates the real decay constants whenever the transition involves a multiplet of closely spaced final states. Considering Equation 24, the semiclassical method and the photon bath will lead to different relative distributions of occupations, affecting the relative amplitudes in the emission spectrum. The difference can be traced back to the mean-field nature of our model, led by the term $\langle\ddot{\mu}\rangle$ in Equation 6. From our results we conclude that the wrong transition rates arise from two effects: the already known fact that Ehrenfest dynamics describes stimulated, as opposed to spontaneous emission; and the incorrect weighting due to the splitting of the final weight among states in the multiplet. This last problem applies to other semiclassical approaches and *ab initio* methods such as MPKS. Real-time dynamics using these models will lead to unphysical results when multiplets of final states are involved. This effect is critical for the study of light-matter interaction and this work is, to our knowledge, the first report of this problem.
Despite the limited accuracy, our semi-classical model includes the same transitions as those predicted by the QED model, and the emission spectrum of the system is easily accessed through the Fourier transform of the dipole moment time-correlation function during the decay process. Even though we expect to obtain an incorrect distribution of spectral amplitudes, we can guarantee that the peaks will be rightly located at the corresponding emission frequencies, without any prior assumption about the nature of the molecular Hamiltonian. We consider this an advantage over the use of QED models in electron dynamics, since the latter does not include electron relaxation nor provides access to the spectral information easily if the eigenvalues of the system are unknown.
We hope that this work will stimulate further studies on the properties and limitations of mean-field light-matter dynamics, which requires application to other radiative phenomena.

ACKNOWLEDGMENTS

This work has been funded by the European Union's Horizon 2020 research and innovation programme through the project ATLANTIC under Grant Agreement No. 823897 and by the Agencia Nacional de Promoción Científica y Tecnológica de Argentina (Grant Nos. PICT 2015-2761 and PICT 2016-3167). A.P.H. acknowledges support from the Thomas Young Centre under Grant No. TYC-101.

Appendix A: Derivation of the master equation based on the Redfield formalism to include a phonon bath

The exact Liouville equation for the evolution of the molecular density operator $\hat{\rho}_{\text{mol}}$ according to the Hamiltonian of Equation 2 is

$$i\hbar\frac{d\hat{\rho}_{\text{mol}}(t)}{dt} = \left[\hat{H}_{\text{mol}}, \hat{\rho}_{\text{mol}}(t)\right] - \sum_k \left[K_0\hat{X}, \hat{\Phi}_k(t)\right] \tag{A1}$$

where $\hat{\Phi}_k(t) = \text{Tr}_{\text{bath}}\{\hat{X}_k\hat{\rho}(t)\}$, being $\hat{\rho}$ the total density operator. In order to get an expression for $\hat{\Phi}_k(t)$ we write the exact

solution for the density

$$\hat{\rho}(t) = e^{-\frac{\mathrm{i}}{\hbar}\hat{H}_0 t}\hat{\rho}(0)e^{\frac{\mathrm{i}}{\hbar}\hat{H}_0 t} - \frac{1}{\mathrm{i}\hbar}\sum_k \int_0^t e^{\frac{\mathrm{i}}{\hbar}\hat{H}_0(\tau-t)}\left[K_0\hat{X}_k\hat{X},\hat{\rho}(\tau)\right]e^{-\frac{\mathrm{i}}{\hbar}\hat{H}_0(\tau-t)}d\tau, \tag{A2}$$

with $\hat{H}_0$ the unperturbed Hamiltonian in the absence of bath-molecule interactions. Now we can write

$$\hat{\Phi}_k(t) = -\frac{K_0}{\mathrm{i}\hbar}\mathrm{Tr}_{\mathrm{bath}}\left\{\sum_{k'}\int_0^t \hat{X}^{\tau-t}\hat{X}_k\hat{X}_{k'}^{\tau-t}\hat{\rho}^{\tau-t}(\tau)d\tau - \int_0^t \hat{\rho}^{\tau-t}(\tau)\hat{X}_{k'}^{\tau-t}\hat{X}_k\hat{X}^{\tau-t}d\tau\right\}, \tag{A3}$$

where we use the notation $\hat{Q}^t = e^{\frac{\mathrm{i}}{\hbar}\hat{H}_0 t}\hat{Q}e^{-\frac{\mathrm{i}}{\hbar}\hat{H}_0 t}$.
We can apply the decomposition $\hat{A}\hat{B} = (1/2)[\hat{A},\hat{B}] + (1/2)\{\hat{A},\hat{B}\}$, to get

$$\hat{\Phi}_k(t) = -\frac{K_0}{2\mathrm{i}\hbar}\mathrm{Tr}_{\mathrm{bath}}\sum_{k'}\int_0^t [\hat{X}^{\tau-t},\hat{\rho}^{\tau-t}(\tau)]\{\hat{X}_k,\hat{X}_{k'}^{\tau-t}\}d\tau - \frac{K_0}{2\mathrm{i}\hbar}\mathrm{Tr}_{\mathrm{bath}}\sum_{k'}\int_0^t \{\hat{X}^{\tau-t},\hat{\rho}^{\tau-t}(\tau)\}[\hat{X}_k,\hat{X}_{k'}^{\tau-t}]d\tau. \tag{A4}$$

Assuming that the bath oscillators are not affected by the molecule, it holds:

$$\sum_{k'}[\hat{X}_k,\hat{X}_{k'}^{\tau-t}] = \frac{\mathrm{i}\hbar}{M\nu_k}\sin(\nu_k(\tau-t)), \tag{A5}$$

$$\mathrm{Tr}_{\mathrm{bath}}\sum_{k'}\left(\{\hat{X}_k,\hat{X}_{k'}^{\tau-t}\}\hat{\rho}_{\mathrm{bath}}^{\tau-t}(\tau)\right) \approx \frac{\hbar}{M\nu_k}(2N_k(\tau)+1)\cos(\nu_k(\tau-t)), \tag{A6}$$

where N_k is the vibrational occupation of the bath-mode k. Finally we get

$$\hat{\Phi}_k(t) = -\frac{K_0}{2\mathrm{i}M\nu_k}\int_0^t [\hat{X}^{\tau-t},\hat{\rho}_{\mathrm{mol}}^{\tau-t}(\tau)](2N_k(\tau)+1)\cos(\nu_k(\tau-t))d\tau - \frac{K_0}{2M\nu_k}\int_0^t \{\hat{X}^{\tau-t},\hat{\rho}_{\mathrm{mol}}^{\tau-t}(\tau)\}\sin(\nu_k(\tau-t))d\tau \tag{A7}$$

To proceed further we make two considerations. First, we take the summation in Equation A1 as an integral on the degrees of freedom of a continuum bath. Second, we use the basis of the vibronic states (i and j). With this in mind, the following matrix elements can be written:

$$\chi_{ij}^{(1)} = \int_{\omega_{\min}}^{\omega_{\max}} -\frac{K_0}{2\mathrm{i}M\nu_k\Delta\omega}(2N_k+1)\int_0^t X_{ij}^{\tau-t}\cos(\nu_k(\tau-t))d\tau\, d\nu_k, \tag{A8}$$

$$\chi_{ij}^{(2)} = \int_{\omega_{\min}}^{\omega_{\max}} -\frac{K_0}{2M\nu_k\Delta\omega}\int_0^t X_{ij}^{\tau-t}\sin(\nu_k(\tau-t))d\tau\, d\nu_k. \tag{A9}$$

The integrals extend between $\omega_{\max}$ and $\omega_{\min}$, the maximum and minimum frequencies of the phonon bath, with $\Delta\omega = \omega_{\max} - \omega_{\min}$, and $\omega_{ij} = \omega_i - \omega_j$, where $\hbar\omega_i$ is one of the eigenvalues of the vibronic system.
The first integral can be rewritten as

$$\chi_{ij}^{(1)} = \int_{\omega_{\min}}^{\omega_{\max}} -\frac{K_0}{2\mathrm{i}M\nu_k\Delta\omega}(2N_k+1)\int_0^t X_{ij}e^{\mathrm{i}\omega_{ij}(\tau-t)}\frac{e^{\mathrm{i}\nu_k(\tau-t)}+e^{-\mathrm{i}\nu_k(\tau-t)}}{2}d\tau\, d\nu_k \tag{A10}$$

and solved by introducing a variable change, $s = \tau - t$, and evaluating the following limits:

$$\begin{aligned}
&\lim_{\varepsilon\to 0^+}\lim_{s\to-\infty}\frac{X_{ij}}{2}\int_s^0 e^{\mathrm{i}(\omega_{ij}+\nu_k-\mathrm{i}\varepsilon)s} + e^{\mathrm{i}(\omega_{ij}-\nu_k-\mathrm{i}\varepsilon)s}ds \\
&= \lim_{\varepsilon\to 0^+}\frac{X_{ij}}{2\mathrm{i}}\left(\frac{1}{\omega_{ij}+\nu_k-\mathrm{i}\varepsilon}+\frac{1}{\omega_{ij}-\nu_k-\mathrm{i}\varepsilon}\right) \\
&= \lim_{\varepsilon\to 0^+}\frac{X_{ij}}{2\mathrm{i}}\left(\frac{\omega_{ij}+\nu_k+\mathrm{i}\varepsilon}{(\omega_{ij}+\nu_k)^2+\varepsilon^2}+\frac{\omega_{ij}-\nu_k+\mathrm{i}\varepsilon}{(\omega_{ij}-\nu_k)^2+\varepsilon^2}\right) \\
&= \frac{X_{ij}}{2\mathrm{i}}\left(\frac{1}{\omega_{ij}+\nu_k}+\frac{1}{\omega_{ij}-\nu_k}+\pi\mathrm{i}\delta(\omega_{ij}+\nu_k)+\pi\mathrm{i}\delta(\omega_{ij}-\nu_k)\right).
\end{aligned} \tag{A11}$$

In this way we can write

$$\chi_{ij}^{(1)} = \int_{\omega_{\min}}^{\omega_{\max}}\frac{X_{ij}K_0(2N_k+1)}{4M\nu_k\Delta\omega}\left(\frac{1}{\omega_{ij}+\nu_k} + \frac{1}{\omega_{ij}-\nu_k}+\pi\mathrm{i}\delta(\omega_{ij}+\nu_k)+\pi\mathrm{i}\delta(\omega_{ij}-\nu_k)\right)d\nu_k. \tag{A12}$$

Operating in the same way for $\chi_{ij}^{(2)}$, from Equation A9 we can get the expression

$$\chi_{ij}^{(2)} = \int_{\omega_{\min}}^{\omega_{\max}}\frac{X_{ij}K_0}{4M\nu_k\Delta\omega}\left(\frac{1}{\omega_{ij}+\nu_k}-\frac{1}{\omega_{ij}-\nu_k} +\pi\mathrm{i}\delta(\omega_{ij}+\nu_k)-\pi\mathrm{i}\delta(\omega_{ij}-\nu_k)\right)d\nu_k. \tag{A13}$$

We neglect the terms related with the Lamb shifts. The remaining terms are easily integrated and produce the required thermalization,

$$\begin{aligned}
\chi_{ij}^{(1)} &\approx \int_{\omega_{\min}}^{\omega_{\max}}\frac{X_{ij}K_0(2N_k+1)}{4M\nu_k\Delta\omega}\left(\pi\mathrm{i}\delta(\omega_{ij}+\nu_k)+\pi\mathrm{i}\delta(\omega_{ij}-\nu_k)\right)d\nu_k \\
&= \frac{\mathrm{i}\pi X_{ij}K_0(2N(|\omega_{ij}|)+1)}{4M|\omega_{ij}|\Delta\omega},
\end{aligned} \tag{A14}$$

$$\chi_{ij}^{(2)} \approx \int_{\omega_{\min}}^{\omega_{\max}} \frac{X_{ij}K_0}{4M\nu_k\Delta\omega}\left(\pi \mathrm{i}\delta(\omega_{ij}+\nu_k)-\pi \mathrm{i}\delta(\omega_{ij}-\nu_k)\right)d\nu_k = -\frac{\mathrm{i}\pi X_{ij}K_0}{4M\omega_{ij}\Delta\omega}, \tag{A15}$$

where $\omega_{\min} < |\omega_{ij}| < \omega_{\max}$ (outside this range the matrix elements are equal to zero). These matrix elements are then employed to form Equation 3.

As an alternative, it is possible to replace the approximations in Equation A14 and A15 by the numerical solutions of the integrals. Nevertheless, this would imply the replacement of the Dirac deltas by a parameterized expression and a finite number of phonons in the bath. This would require a preliminary calibration process preceding the simulations[23].

Equation 3 can also be expressed in the standard form of the Redfield equation

$$\frac{d\sigma_{ij}(t)}{dt} = -\mathrm{i}\omega_{ij}\sigma_{ij}(t) + \sum_{kl} R_{ijkl}\sigma_{kl}(t). \tag{A16}$$

Here $\sigma_{ij}(t) = \langle i|\hat{\rho}_{\mathrm{mol}}(t)|j\rangle$, and R_{ijkl} is the Redfield tensor

$$R_{ijkl} = \Gamma^{+}_{ljik} + \Gamma^{-}_{ljik} - \delta_{jl}\sum_m \Gamma^{+}_{immk} - \delta_{ik}\sum_m \Gamma^{-}_{lmmj}. \tag{A17}$$

Using our derivation, it is possible to write this terms in function of the elements $\chi_{ij}^{(1)}$ and $\chi_{ij}^{(2)}$

$$\Gamma^{+}_{ljik} = \frac{1}{\mathrm{i}\hbar}X_{lj}\left(\chi^{(1)}_{ik}+\chi^{(2)}_{ik}\right), \qquad \Gamma^{-}_{ljik} = \frac{1}{\mathrm{i}\hbar}X_{ik}\left(\chi^{(1)}_{lj}-\chi^{(2)}_{lj}\right). \tag{A18}$$

We chose to use the expression shown in Equation 3 in the main text for its simplicity and generality.

Appendix B: Derivation of the master equation based on the Redfield formalism to include a photon bath

We define the unit vector from Equation 11, $\boldsymbol{\epsilon}_{\mathbf{k},\lambda} = (\varepsilon^x_{\mathbf{k},\lambda}, \varepsilon^y_{\mathbf{k},\lambda}, \varepsilon^z_{\mathbf{k},\lambda})$, to satisfy the next conditions

$$\boldsymbol{\epsilon}_{\mathbf{k},1} = \frac{\mathbf{e_1}\times\mathbf{k}}{|\mathbf{e_1}\times\mathbf{k}|}, \qquad \boldsymbol{\epsilon}_{\mathbf{k},2} = \boldsymbol{\epsilon}_{\mathbf{k},1}\times\frac{\mathbf{k}}{|\mathbf{k}|}, \tag{B1}$$

where $\mathbf{e_1}$ is the unit vector in the x direction. This conditions help us to simplify the expression of the interaction term if we consider that $\hat{\boldsymbol{\mu}} = \hat{\mu}_x\mathbf{e_1}$

$$\hat{\mathbf{E}}_{\mathbf{k}}\cdot\hat{\boldsymbol{\mu}} = \hat{E}^x_{\mathbf{k}}\hat{\mu}_x = -\mathrm{i}\,\varepsilon^x_{\mathbf{k},2}\left(\frac{\hbar\omega_{\mathbf{k}}}{2\varepsilon_0 V}\right)^{1/2}(\hat{a}^\dagger_{\mathbf{k}}-\hat{a}_{\mathbf{k}})\hat{\mu}_x, = -\mathrm{i}\frac{(k_z^2+k_y^2)^{1/2}}{|\mathbf{k}|}\left(\frac{\hbar\omega_{\mathbf{k}}}{2\varepsilon_0 V}\right)^{1/2}(\hat{a}^\dagger_{\mathbf{k}}-\hat{a}_{\mathbf{k}})\hat{\mu}_x. \tag{B2}$$

For sake of simplicity, we ignored the λ index from $\hat{a}^\dagger_{\mathbf{k}}$ and $\hat{a}_{\mathbf{k}}$ operators. Again, we use the Liouville equation

$$\mathrm{i}\hbar\frac{d\hat{\rho}_{\mathrm{mol}}(t)}{dt} = [\hat{H}_{\mathrm{mol}}, \hat{\rho}_{\mathrm{mol}}(t)] - \sum_{\mathbf{k}}[\hat{\mu}_x, \hat{\Phi}_{\mathbf{k}}(t)] \tag{B3}$$

where $\hat{\Phi}_{\mathbf{k}}(t) = \mathrm{Tr}_{\mathrm{bath}}\{\hat{E}^x_{\mathbf{k}}\rho(t)\}$, and now the trace is over the photon modes. Henceforth, we will replace $\hat{E}^x_{\mathbf{k}}$ and $\hat{\mu}_x$ by $\hat{E}_{\mathbf{k}}$ and $-e\hat{x}$ respectively. The exact solution of the density is

$$\hat{\rho}(t) = e^{-\frac{\mathrm{i}}{\hbar}\hat{H}_0 t}\hat{\rho}(0)e^{\frac{\mathrm{i}}{\hbar}\hat{H}_0 t} + \frac{1}{\mathrm{i}\hbar}\sum_{\mathbf{k}}\int_0^t e^{\frac{\mathrm{i}}{\hbar}\hat{H}_0(\tau-t)}[e\hat{E}_{\mathbf{k}}\hat{x}, \hat{\rho}(\tau)]e^{-\frac{\mathrm{i}}{\hbar}\hat{H}_0(\tau-t)}d\tau, \tag{B4}$$

where we are using the same notation as in Appendix A, and following the same steps we get

$$\hat{\Phi}_{\mathbf{k}}(t) = \frac{e}{2\mathrm{i}\hbar}\mathrm{Tr}_{\mathrm{bath}}\sum_{\mathbf{k}'}\int_0^t [\hat{x}^{\tau-t}, \hat{\rho}^{\tau-t}(\tau)]\{\hat{E}_{\mathbf{k}}, \hat{E}^{\tau-t}_{\mathbf{k}'}\}d\tau + \frac{e}{2\mathrm{i}\hbar}\mathrm{Tr}_{\mathrm{bath}}\sum_{\mathbf{k}'}\int_0^t \{\hat{x}^{\tau-t}, \hat{\rho}^{\tau-t}(\tau)\}[\hat{E}_{\mathbf{k}}, \hat{E}^{\tau-t}_{\mathbf{k}'}]d\tau. \tag{B5}$$

Making similar assumptions to those we made for the case of the phonon bath, we can use

$$\sum_{\mathbf{k}'}[\hat{E}_{\mathbf{k}}, \hat{E}^{\tau-t}_{\mathbf{k}'}] = \mathrm{i}\frac{k_z^2+k_y^2}{|\mathbf{k}|^2}\frac{\hbar\omega_{\mathbf{k}}}{\varepsilon_0 V}\sin(\omega_{\mathbf{k}}(\tau-t)), \tag{B6}$$

and the approximation

$$\mathrm{Tr}_{\mathrm{bath}}\sum_{\mathbf{k}'}\left(\{\hat{E}_{\mathbf{k}}, \hat{E}^{\tau-t}_{\mathbf{k}'}\}\hat{\rho}^{\tau-t}_{\mathrm{bath}}(\tau)\right) \approx \frac{k_z^2+k_y^2}{|\mathbf{k}|^2}\frac{\hbar\omega_{\mathbf{k}}}{\varepsilon_0 V}(2N_{\mathbf{k}}(\tau)+1)\cos(\omega_{\mathbf{k}}(\tau-t)), \tag{B7}$$

to finally get

$$\hat{\Phi}_{\mathbf{k}}(t) = \frac{e\omega_{\mathbf{k}}}{2\mathrm{i}\varepsilon_0 V}\frac{k_z^2+k_y^2}{|\mathbf{k}|^2}\int_0^t [\hat{x}^{\tau-t}, \hat{\rho}^{\tau-t}_{\mathrm{mol}}(\tau)](2N_{\mathbf{k}}(\tau)+1)\cos(\omega_{\mathbf{k}}(\tau-t))d\tau + \frac{e\omega_{\mathbf{k}}}{2\varepsilon_0 V}\frac{k_z^2+k_y^2}{|\mathbf{k}|^2}\int_0^t \{\hat{x}^{\tau-t}, \hat{\rho}^{\tau-t}_{\mathrm{mol}}(\tau)\}\sin(\omega_{\mathbf{k}}(\tau-t))d\tau. \tag{B8}$$

As before, we replace the summation of the photon modes with an integral and we define the following matrix elements

$$\chi_{ij}^{(1)} = \int_0^\infty \frac{e\omega_{\mathbf{k}}^3}{6\mathrm{i}\pi^2\varepsilon_0 c^3}(2N_{\mathbf{k}}+1)\int_0^t x_{ij}^{\tau-t}\cos(\omega_{\mathbf{k}}(\tau-t))d\tau\, d\omega_{\mathbf{k}}, \tag{B9}$$

$$\chi_{ij}^{(2)} = \int_0^\infty \frac{e\omega_{\mathbf{k}}^3}{6\pi^2\varepsilon_0 c^3}\int_0^t x_{ij}^{\tau-t}\sin(\omega_{\mathbf{k}}(\tau-t))d\tau\, d\omega_{\mathbf{k}}. \tag{B10}$$

The integrals in function of time can be solved in the same way as in the Appendix A. Here we also ignore the terms related to the Lamb shift, and we finally get the expressions

$$\chi_{ij}^{(1)} \approx -\int_0^\infty \frac{e x_{ij}\omega_{\mathbf{k}}^3}{12\pi^2\varepsilon_0 c^3}(2N_{\mathbf{k}}+1)\left(\pi \mathrm{i}\delta(\omega_{ij}+\omega_{\mathbf{k}})+\pi \mathrm{i}\delta(\omega_{ij}-\omega_{\mathbf{k}})\right)d\omega_{\mathbf{k}} = -\frac{\mathrm{i}\,e x_{ij}|\omega_{ij}|^3}{12\pi\varepsilon_0 c^3}(2N(|\omega_{ij}|)+1), \tag{B11}$$

$$\chi_{ij}^{(2)} \approx -\int_0^\infty \frac{e x_{ij}\omega_{\mathbf{k}}^3}{12\pi^2\varepsilon_0 c^3}\left(\pi \mathrm{i}\delta(\omega_{ij}+\omega_{\mathbf{k}}) - \pi\mathrm{i}\delta(\omega_{ij}-\omega_{\mathbf{k}})\right) d\omega_{\mathbf{k}} = \frac{\mathrm{i}\, e x_{ij}\omega_{ij}^3}{12\pi\varepsilon_0 c^3}. \tag{B12}$$

Appendix C: CEED derivation

Here we show that CEED is a mean-field theory. In the Coulomb gauge we have[24]

$$\nabla^2\phi = -\frac{\rho}{\varepsilon_0}$$
$$\left(\nabla^2 - \frac{1}{c^2}\frac{\partial^2}{\partial t^2}\right)\vec{A} = -\frac{1}{c^2\varepsilon_0}\vec{j}^{\perp} \tag{C1}$$

where ρ is the charge density, ε_0 is the permittivity of free space, c is the speed of light, and $\vec{j}^{\perp}$ is the transverse component of the current density and satisfies $\vec{\nabla}\cdot\vec{j}^{\perp} = 0$. This has the solution

$$\vec{A}(\vec{r}t) = -\frac{e\mu_0}{4\pi}\int \frac{\vec{j}^{\perp}\left(\vec{r}', t - \frac{1}{c}|\vec{r}'-\vec{r}|\right)}{|\vec{r}'-\vec{r}|}\,\mathrm{d}\vec{r}' \tag{C2}$$

If we associate the term involving ϕ with the usual Coulomb interaction between electrons, then we can make it part of the electronic Hamiltonian. The free field Hamiltonian H_p then just depends on the vector potential

$$H_p(\vec{A}) = \frac{1}{2}\int\left(\frac{1}{\varepsilon_0}\vec{\Pi}^2 + \varepsilon_0 c^2\left(\vec{\nabla}\times\vec{A}\right)^2\right)\mathrm{d}\vec{r} \tag{C3}$$

where $\vec{\Pi} = \varepsilon_0\frac{\partial\vec{A}}{\partial t}$ is the momentum conjugate to $\vec{A}$.

Now let us consider the coupled system of electrons and electromagnetic fields. Let $\vec{x}_i$ represent the position of electron i and $\vec{p}_i$ be the corresponding momentum. The Hamiltonian $\hat{H}$ describing the interacting system of electrons and photons then has the form

$$\hat{H} = \hat{H}_e(\{\hat{\vec{x}}_i, \hat{\vec{p}}_i\}) + \hat{H}_p(\hat{\vec{A}}) + \hat{H}_{ep}(\{\hat{\vec{x}}_i, \hat{\vec{p}}_i\}, \hat{\vec{A}}) \tag{C4}$$

where we have replaced classical variables with quantum operators. Here $\hat{H}_e$ is the electronic Hamiltonian, $\hat{H}_p$ is the photonic Hamiltonian and $\hat{H}_{ep}$ is the interaction Hamiltonian. The quantum Liouville equation for the interacting system is then

$$\mathrm{i}\hbar\frac{\partial\hat{\rho}_S}{\partial t} = \left[\hat{H}, \hat{\rho}_S\right] \tag{C5}$$

where $\hat{\rho}_S$ is the density matrix for the whole system (electrons and photons). If we trace out the photons we get an equation for an electronic density matrix $\hat{\rho} = \mathrm{Tr}_p\{\hat{\rho}_S\}$

$$\mathrm{i}\hbar\frac{\partial\hat{\rho}}{\partial t} = \left[\hat{H}_e, \hat{\rho}\right] + \mathrm{Tr}_p\left\{\left[\hat{H}_{ep}, \hat{\rho}_S\right]\right\} \tag{C6}$$

We shall keep just the term in the interaction Hamiltonian that is linear $\vec{A}$

$$\hat{H}_{ep} = e\int \hat{\vec{j}}(\vec{r})\cdot\hat{\vec{A}}(\vec{r})\,\mathrm{d}\vec{r} \tag{C7}$$

where

$$\hat{\vec{j}}(\vec{r}) = \frac{1}{2m}\sum_i\left(\hat{\vec{p}}_i\delta\left(\vec{r}-\hat{\vec{x}}_i\right) + \delta\left(\vec{r}-\hat{\vec{x}}_i\right)\hat{\vec{p}}_i\right) \tag{C8}$$

The core approximation we now make is the mean field ansatz

$$\hat{\rho}_S = \hat{\rho}\otimes\hat{\rho}_p \tag{C9}$$

where $\hat{\rho}_p$ is the photon density matrix. From this we get

$$\mathrm{i}\hbar\frac{\partial\hat{\rho}}{\partial t} = \left[\hat{H}_e + \left\langle\hat{H}_{ep}\right\rangle_p, \hat{\rho}\right] \tag{C10}$$

where

$$\left\langle\hat{H}_{ep}\right\rangle_p = \mathrm{Tr}_p\left\{\hat{H}_{ep}\hat{\rho}_p\right\} = e\int\hat{\vec{j}}(\vec{r})\cdot\vec{A}(\vec{r})\,\mathrm{d}\vec{r} \tag{C11}$$

and

$$\vec{A}(\vec{r}) = \mathrm{Tr}_p\left\{\hat{\vec{A}}(\vec{r})\hat{\rho}_p\right\}$$
$$\vec{j}(\vec{r}) = \mathrm{Tr}_e\left\{\hat{\vec{j}}(\vec{r})\hat{\rho}\right\} \tag{C12}$$

If we substitute Eq. C8 into Eq. C11 we get

$$\left\langle\hat{H}_{ep}\right\rangle_p = \frac{e}{2m}\sum_i\left(\hat{\vec{p}}_i\cdot\vec{A}(\hat{\vec{x}}_i) + \vec{A}(\hat{\vec{x}}_i)\cdot\hat{\vec{p}}_i\right) \tag{C13}$$

If retardation effects are small, we can approximate Eq. C2 by

$$\vec{A}(\vec{r}t) \approx \vec{A}_0(\vec{r}t) + \vec{A}_1(\vec{r}t) \tag{C14}$$

where

$$\vec{A}_0(\vec{r}t) = -\frac{e\mu_0}{4\pi}\int\frac{\vec{j}^{\perp}(\vec{r}', t)}{|\vec{r}'-\vec{r}|}\,\mathrm{d}\vec{r}'$$
$$\vec{A}_1(\vec{r}t) = \frac{e\mu_0}{4\pi c}\frac{\partial}{\partial t}\int\vec{j}^{\perp}\left(\vec{r}', t\right)\mathrm{d}\vec{r}' \tag{C15}$$

We can identify $\vec{A}_0(\vec{r}t)$ with the non-radiating magnetic field, thus we will only consider the contribution from $\vec{A}_1(\vec{r}t)$. From Eqs. C12 and C8 we get

$$\int\vec{j}^{\perp}(\vec{r})\,\mathrm{d}\vec{r} = \frac{2}{3}\frac{1}{m}\sum_i\mathrm{Tr}_e\left\{\hat{\vec{p}}_i\hat{\rho}\right\} = \frac{2}{3}\sum_i\dot{\vec{x}}_i \tag{C16}$$

where

$$\vec{x}_i = \mathrm{Tr}_e\left\{\hat{\vec{x}}_i\hat{\rho}\right\} \tag{C17}$$

Substituting Eq. C16 into Eq. C15 gives

$$e\vec{A}_1(\vec{r}t) = \frac{2}{3}\frac{\alpha\hbar}{c^2}\sum_i\ddot{\vec{x}}_i \tag{C18}$$

where α is the fine structure constant. If we argue that radiation is a result of dipolar terms ($\vec{A}_1$ is uniform over the molecule), then Eq. C13 can be simplified to

$$\left\langle\hat{H}_{ep}\right\rangle_p^{radiation} = \frac{2\alpha\hbar}{3c^2}\sum_{ij}\frac{\hat{\vec{p}}_j}{m}\cdot\ddot{\vec{x}}_i \tag{C19}$$

[1]P. Atkins, P. W. Atkins, and J. de Paula, *Atkins' physical chemistry* (Oxford University Press, 2014).
[2]B. F. Curchod and T. J. Martínez, Chem. Rev. **118**, 3305–3336 (2018).
[3]F. Agostini and B. F. Curchod, Wiley Interdiscip. Rev. Comput. Mol. Sci. **9**, e1417 (2019).
[4]F. Ramírez, G. Díaz Mirón, M. C. González Lebrero, and D. A. Scherlis, Theor. Chem. Acc. **137**, 1–9 (2018).
[5]G. Díaz Mirón and M. C. Gonzaález Lebrero, J. Phys. Chem. A **124**, 9503–9512 (2020).
[6]Y. Tanimura, J. Chem. Phys. **153**, 020901 (2020).
[7]M. Sánchez-Barquilla and J. Feist, Nanomaterials **11**, 2104 (2021).
[8]F. Di Maiolo and A. Painelli, J. Chem. Theory Comput. **14**, 5339–5349 (2018).
[9]C. Chuang and P. Brumer, J. Phys. Chem. Lett. **12**, 3618–3624 (2021).
[10]C. Chuang and P. Brumer, J. Phys. Chem. Lett. **13**, 4963–4970 (2022).
[11]D. Giavazzi, F. Di Maiolo, and A. Painelli, Phys. Chem. Chem. Phys. **24**, 5555–5563 (2022).
[12]D. Jadoun and M. Kowalewski, J. Phys. Chem. Lett. **12**, 8103–8108 (2021).
[13]M. Ruggenthaler, J. Flick, C. Pellegrini, H. Appel, I. V. Tokatly, and A. Rubio, Phys. Rev. A **90**, 012508 (2014).
[14]J. Flick, C. Schäfer, M. Ruggenthaler, H. Appel, and A. Rubio, ACS photonics **5**, 992–1005 (2018).
[15]T. S. Haugland, E. Ronca, E. F. Kjø nstad, A. Rubio, and H. Koch, Phys. Rev. X **10**, 041043 (2020).
[16]T. E. Li, H.-T. Chen, and J. E. Subotnik, J. Chem. Theory Comput. **15**, 1957–1973 (2019).
[17]H.-T. Chen, T. E. Li, M. Sukharev, A. Nitzan, and J. E. Subotnik, J. Chem. Phys. **150**, 044102 (2019).
[18]C. M. Bustamante, E. D. Gadea, A. Horsfield, T. N. Todorov, M. C. G. Lebrero, and D. A. Scherlis, Phys. Rev. Lett. **126**, 087401 (2021).
[19]E. D. Gadea, C. M. Bustamante, T. N. Todorov, and D. A. Scherlis, Phys. Rev. A **105**, 042201 (2022).
[20]R. Jestädt, M. Ruggenthaler, M. J. Oliveira, A. Rubio, and H. Appel, Adv. Phys. **68**, 225–333 (2019).
[21]A. G. Redfield, IBM J. Res. Dev. **1**, 19–31 (1957).
[22]D. A. McQuarrie, *Statistical Mechanics* (University Science Books, 2000).
[23]C. M. Bustamante, T. N. Todorov, C. G. Sánchez, A. Horsfield, and D. A. Scherlis, J. Chem. Phys. **153**, 234108 (2020).
[24]D. P. Craig and T. Thirunamachandran, *Molecular quantum electrodynamics: an introduction to radiation-molecule interactions* (Courier Corporation, 1998).